Climate
of the Past

Discussions

CO₂ and summer insolation as drivers for the Mid-Pleistocene transition

Meike D. W. Scherrenberg[1], Constantijn J. Berends[1], Roderik S.W. van de Wal[1,2]

[1]Institute for Marine and Atmospheric research Utrecht, Utrecht University, Utrecht, the Netherlands
[2]Faculty of Geosciences, Department of Physical Geography, Utrecht University, Utrecht, the Netherlands

Correspondence to: M.D.W. Scherrenberg (M.D.W.Scherrenberg@uu.nl)

During the Mid-Pleistocene transition (MPT) the dominant periodicity of glacial cycles increased from 41 thousand years (kyr) to an average of 100 kyr, without any appreciable change in the orbital pacing. As the MPT is not a linear response to orbital forcing, it must have resulted from feedback processes in the Earth system. However, the precise mechanisms underlying the transition are still under debate.

In this study, we investigate the MPT by simulating the Northern Hemisphere ice sheet evolution over the past 1.5 million years. The transient climate forcing of the ice-sheet model was obtained using a matrix method, by interpolating between two snapshots of global climate model simulations. Changes in climate forcing are caused by variations in CO_2, insolation, as well as implicit climate–ice sheet feedbacks.

Using this method, we were able to capture glacial-interglacial variability during the past 1.5 million years and reproduce the shift from 41 kyr to 100 kyr cycles without any additional drivers. Instead, the modelled frequency change results from the prescribed CO_2 combined with orbital forcing, and ice sheet feedbacks. Early Pleistocene terminations are initiated by insolation maxima. After the MPT, low CO_2 levels can compensate insolation maxima which favour deglaciation, leading to an increasing glacial cycle periodicity. These deglaciations are also prevented by a relatively small North American ice sheet, which, through its location and feedback processes, can generate a relatively stable climate. Larger North American ice sheets become more sensitive to small temperature increases. Therefore, Late Pleistocene terminations are facilitated by the large ice-sheet volume, were small changes in temperature lead to self-sustained melt instead.

This concept is confirmed by experiments using constant insolation or CO_2. The constant CO_2 experiments generally capture only the Early Pleistocene cycles, while those with constant insolation only capture Late Pleistocene cycles. Additionally, we find that a lowering of CO_2 concentrations leads to an increasing number of insolation maxima that fail to initiate terminations. These results therefore suggest a regime shift, where during the Early Pleistocene, glacial cycles are dominated by orbital oscillations, while Late Pleistocene cycles tend to be more dominated by CO_2. This implies that the MPT can be explained by a decrease in glacial CO_2 concentration superimposed on orbital forcing.

Climate
of the Past
Discussions

1. Introduction

During the Mid-Pleistocene transition (MPT; ~1.2 – 0.8 million years ago) the duration of glacial cycles shifted from 41 kyr to an average of 100 kyr, but the main mechanisms behind this change are still under debate. Glacial cycles are paced by orbital cycles, namely precession (~19/23 kyr), obliquity (~41 kyr), and eccentricity (~98/400 kyr), which determine the latitudinal

35 and seasonal distribution of solar radiation received by the Earth. Ice sheets are especially sensitive to summer insolation, as regions may undergo melt and a small change in temperature or insolation can strongly alter melt rates. As a result, the 41 kyr periodicity during the Early Pleistocene (2580 – 800 kyr ago) mostly follows the obliquity cycle (e.g., Huybers and Tziperman, 2008; Tabor et al., 2015; Watanabe et al., 2023), but the mechanisms behind the average 100 kyr periodicity of the Late Pleistocene (800 – 11 kyr ago) are more difficult to explain. It has been suggested that the 100 kyr periodicity is a non-linear

40 response to predominantly obliquity (e.g., Huybers and Wunsch, 2005), precession and eccentricity (e.g., Lisiecki, 2010; Hobart, et al. 2023; Blackburn et al., 2024), or a combination of orbital cycles (e.g., Huybers, 2011; Feng and Bailer-Jones, 2015; Tzedakis, et al. 2017). Nevertheless, the transition from 41 kyr to 100 kyr glacial cycles took place without any considerable change in the orbital cycles, and it must therefore have resulted from feedback processes within the Earth's system.

45 One overarching hypothesis for the MPT suggest that the ice sheets display a threshold regime (see Berends, et al. 2021a; Paillard, 1998). Small or flat ice sheets can easily melt at insolation maxima. Medium-sized ice sheets may survive insolation maxima due to albedo and topography feedbacks, facilitating low temperatures in glaciated regions. Large ice sheets become vulnerable through positive feedbacks such as the elevation-temperature feedback, albedo feedbacks, and high basal temperatures enhancing sliding (Bintanja and van de Wal, 2008), and Proglacial Ice Sheet Instability (PLISI; see Hinck et al.,

50 2022; Quiquet et al., 2021; Scherrenberg et al., 2024). This is further supported by several studies showing that the Late Pleistocene glacial cycles only melt once they reach a certain ice volume (Abe-Ouchi et al., 2013; Parrenin and Paillard, 2003; Bintanja and van de Wal, 2008; Berends et al., 2021a).

Alternatively, it has been suggested that the MPT is caused by regolith removal, as first proposed by Clark and Pollard (1998). The regolith hypothesis states that sediments covered North America during the Early Pleistocene. Sediments are easily

55 deformed and enhance sliding, creating flatter ice sheets with relatively larger ablation areas. Ice sheets superimposed on sediments are therefore more vulnerable to small changes in forcing. Once this sediment was removed by the erosive action of the ice sheet, friction increased, reducing ice sheet flow. This produces thicker ice sheets that may survive insolation maxima. Several modelling studies were dedicated to this regolith hypothesis and were able to capture characteristics of the MPT (e.g., Tabor and Poulsen 2016, Ganopolski and Calov, 2011; Mitsui et al., 2023). Recently, Willeit et al. (2019) used a coupled

60 climate-ice-sheet-carbon-cycle model and was able to reproduce the MPT using prescribed gradual atmospheric CO_2 and regolith removal. The regolith theory is also supported by geological data which show a change in the composition of glacial sediments (e.g., Roy et al., 2004; Portier et al., 2021).

Alternative explanations argue that the carbon cycle instead plays a major role in controlling the transition from 41 kyr to 100 kyr glacial cycles. During the Late Pleistocene glacial cycles, glacial-interglacial variations in CO_2 were roughly 90 ppm. (Bereiter et al., 2015). This variation in CO_2 can be largely attributed to the ocean (e.g., Sigman and Boyle, 2000; Brovkin et al., 2012). During glacial periods, CO_2 solubility increases due to lower ocean temperatures, which is further enhanced by increased alkalinity (Kurahashi-Nakamura et al., 2010; Sigman et al., 2010). Glacial-erosional and enhanced dust concentrations in the atmosphere provides nutrients to the Southern Ocean. This increases the biological productivity (Martin, 1990; Martínez-García et al. 2014; Chalk et al., 2017; Saini et al., 2023) and eventually leads to more uptake of CO_2 in the deep-ocean. Additionally, decreased deep-ocean ventilation during glacial periods may have more efficiently trapped carbon (Hasenfratz et al., 2019), which could be explained by increased sea ice extent (Menviel, 2019), or enhanced ocean stratification (Bouttes et al., 2009; Adkins, 2013; Qin et al., 2022). These processes in the carbon cycle are important for decreasing CO_2 levels in the atmosphere during Late Pleistocene glacial periods, but perhaps they also played a crucial role during the MPT. After the MPT, glacial CO_2 concentrations may have dropped due to increased deep-ocean carbon storage (Köhler and Bintanja, 2008; Lear et al., 2016; Farmer et al., 2019; Thomas et al., 2022; Qin et al., 2022) which could have resulted from increased Antarctic bottom water formation due to a change in circulation (e.g., Pena et al., 2014), or an increase in sea ice extent (Detlef et al., 2018).

Nevertheless, despite the complexity and uncertainties in the carbon cycle, atmospheric CO_2 can be measured from ice cores (e.g. Bereiter et al. 2015), or estimated through proxies (e.g. Hönisch et al., 2009; Da et al., 2019; Dyez et al., 2018; Yamamoto et al., 2022). Ice core CO_2 records tend to have low uncertainties but the current oldest continuous record dates back to only 800 kyr ago (Bereiter et al., 2015), which does not capture the MPT. Other CO_2 records can provide us information by indirectly measuring signals controlled by CO_2 variations, though at the expense of higher uncertainty. For example, recently Yamamoto et al. (2022) published a continuous 1.5-million-year CO_2 record based on a leaf-wax indicator.

In this study, we simulate the past 1.5 million years using an ice-sheet model without any change in model set-up over time, and a constant sediment mask. Our main goal is to explore if we can simulate the MPT, and the possible mechanisms behind it, based on only CO_2 and insolation variations. The purpose is therefore not to make perfect spatial reconstructions, but rather to explain the frequency change of glacial-interglacial variability. To provide the model with information on climate, we use a matrix method which is based on interpolated 2D-time-slices from general circulation models (GCM). The temporal climate interpolation is driven by prescribed CO_2 and insolation (see Berends et al., 2018; Scherrenberg et al., 2024). Here we use the CO_2 levels from Yamamoto et al. (2022), which yields us the opportunity to prescribe CO_2 concentrations during the MPT. This method allows us to provide transient climate forcing at a significantly reduced computational time compared to GCM's or intermediate complexity models (e.g., Ganopolski and Calov, 2011; Willeit et al., 2019). Temperature change is mainly driven by prescribed CO_2 records from leaf-wax proxy (1450-0 kyr ago) or ice cores (800-0 kyr ago), combined with caloric summer half-year insolation (Tzedakis et al. 2017). To establish the effect of CO_2 and insolation variations on glacial-interglacial time-scales, we run the same 1450 kyr experiments with constant CO_2 or insolation levels.

Climate
of the Past
Discussions

2. Methods

To simulate ice-sheet evolution during the past 1.5 million years, we use the vertically integrated ice-sheet model IMAU-ICE version 2.1 (Berends et al., 2022). North America, Eurasia and Greenland are simulated in separate model domains, which are shown in Fig. 1.
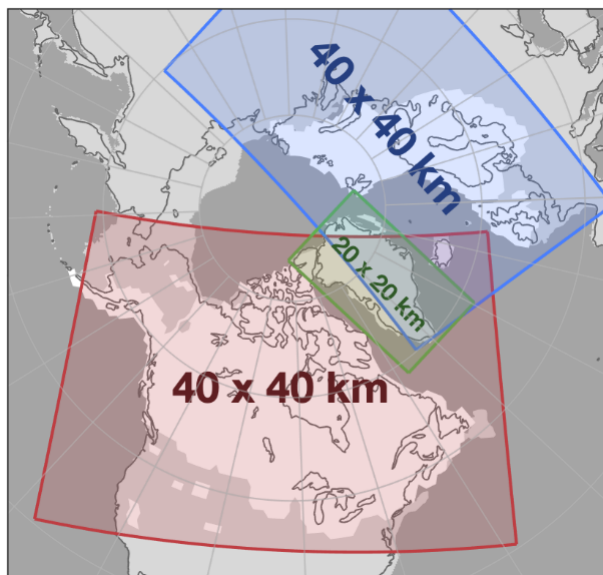
Figure 1. The extent and resolution of the ice-sheet model domains: North America (red), Greenland (green) and Eurasia (blue). For reference, the ICE-6G LGM ice sheet of Peltier et al. (2015) is shown in white. Ice in overlapping regions is removed (e.g., Greenland in the North American domain).

The flow of ice is calculated using the shallow ice / shallow shelf approximation (Bueler and Brown, 2009). Basal hydrology is based on Martin et al. (2011). To calculate basal friction, we apply a present-day sediment map for North America (Gowan et al., 2019), and, as this map does not cover Eurasia, we generate a friction map for this continent using the sediment thickness by Laske and Masters (1997). While sediment distribution may have changed through transport and erosion, we keep a constant sediment map to test whether it is possible to capture the MPT without any changes in basal friction.

To simulate bedrock changes due to ice sheet load, we use an Elastic Lithosphere, Relaxing Asthenosphere model (Le Meur and Huybrechts, 1996). If bedrock topography is below sea level, it is considered as ocean or lake. At the grounding line we include a sub-grid friction scaling scheme based on Leguy et al. (2021) and Feldmann et al. (2014). Ice is removed if the thickness at the calving front is below 200 m. Additionally, floating ice beyond the continental shelf is always removed. To calculate basal melt, we use a depth dependent sub-shelf parameterization based on Martin et al. (2011). Ocean temperatures are based on de Boer et al. (2013), and while they evolve over time, they do not vary spatially within a model domain. For the surface mass balance (SMB), we use IMAU-ITM (insolation, temperature model), which includes a melt parameterization (Bintanja et al., 2002) that depends on temperature, albedo and insolation, a snow-rain partitioning scheme (Ohmura et al.,

100

105

110

115

1999), and a refreezing scheme (Huybrechts and de Wolde, 1999). IMAU-ITM has been shown to be perform well for present-day Greenland conditions (see Fettweis et al., 2020).

2.1 Climate forcing

120 To calculate the transient climate forcing over the past 1.5 million years, we interpolate between GCM-calculated climates of pre-industrial (PI) and the Last Glacial Maximum (LGM). Since the choice of GCM climates can cause large differences in the modelled ice sheets (Alder and Hostetler, 2019; Niu et al., 2019; Scherrenberg et al., 2023), we use a climate ensemble obtained from the Paleoclimate Modelling Intercomparison Project (PMIP4; Kageyama et al., 2017, 2018) rather than a large quantity of time-slices from a single model. The four simulations that had all data necessary for our simulations are MIROC
125 (Ohgaito et al., 2021), MPI (Mauritsen et al., 2019), AWI (Shi et al., 2023) and INM (Volodin et al., 2018). Differences in topography between climate and ice-sheet model are accounted for by applying a lapse rate correction for temperature, and by applying a correction for precipitation with wind-ward and leeward topography effects based on the approach by Roe and Lindzen (2001). The technical details of these methods are described in Scherrenberg et al. (2023).

To interpolate the climate time-slices through time we use a matrix method (see Berends et al., 2018; Scherrenberg
130 et al., 2023; Scherrenberg et al., 2024). Equations governing the matrix method are described in Appendix A. Here we provide a brief, qualitative summary.
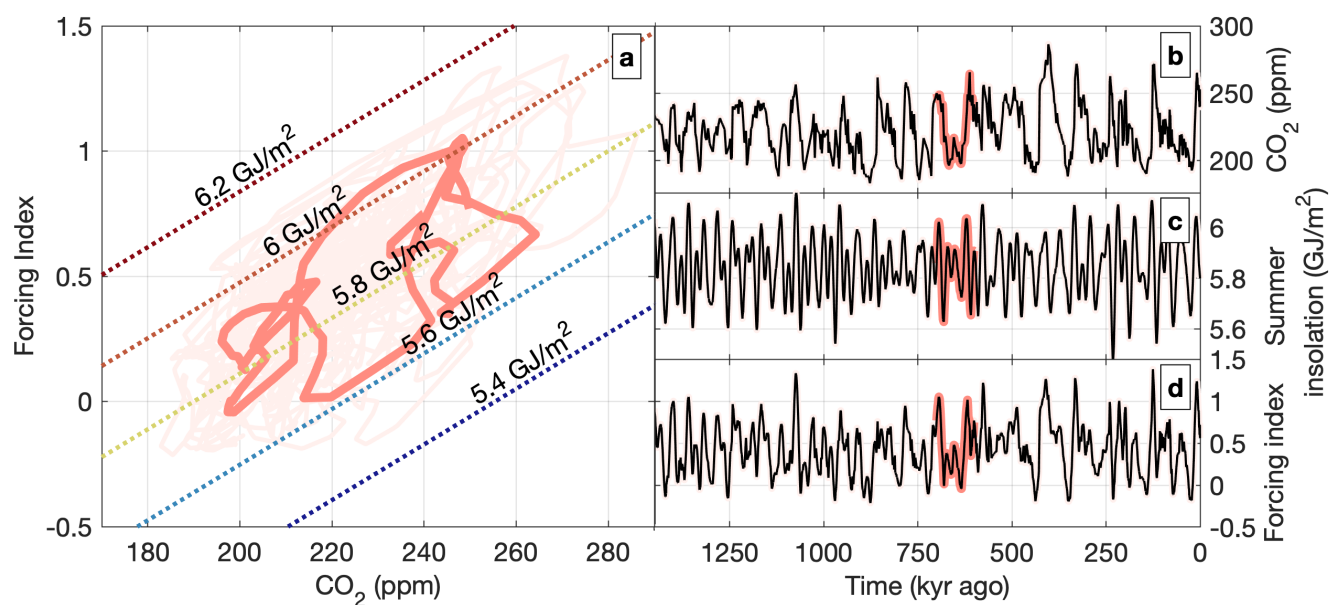

Figure 2. The forcing index (a,d) is a combination of CO_2 (b; x-axis in a) and caloric summer-half year insolation at 65°N (c; diagonal lines in a). Red shows the evolution of the forcing index over one glacial cycle, while pink (see panel a) shows the forcing index over the entire
135 simulation.

Climate
of the Past

Discussions

Temperature depends on the prescribed external forcing (CO_2 and summer insolation) and the modelled ice-sheet, to create a first-order approximation of the ice-albedo feedback. Fig. 2 shows how the prescribed CO_2 and caloric summer insolation (Tzedakis et al. 2017) are combined to calculate the external forcing index. To approximate the albedo feedback, we follow the approach by Berends et al. (2018), where the monthly/latitudinally varying insolation is multiplied with the modelled albedo to yield the 'absorbed insolation'. As the modelled albedo depends on the modelled ice-sheet extent and snow cover, this introduces the feedback from the ice sheet back onto the climate.

Precipitation is modelled similarly, but there the ice-sheet term relates to the (modelled, local) ice thickness rather than the extent, in order to approximate the plateau desert effect. A geometry-based correction, which includes the orographic forcing of precipitation by upslope winds (Roe and Lindzen, 2001), helps to more accurately track the higher precipitation rates at the (moving) ice margin.

2.2 Benthic $\delta^{18}O$

Challenges in studying the MPT are the large uncertainties in sea level reconstructions, especially during the Early Pleistocene. The benthic $\delta^{18}O$ record contains the combined signals of ice volume and deep-water temperature, which are difficult to disentangle. To validate our results, we simulate benthic $\delta^{18}O$ by modelling a separate contribution from deep-water temperature and ice volume.

IMAU-ICE includes a $\delta^{18}O$ model based on the approach by de Boer et al. (2013). This approach uses a depth-integrated advection solver to calculate the evolution of the englacial isotope content, which is forced at the surface by an elevation-dependent parameterisation following Clarke et al. (2005). The governing equations of this approach are detailed in appendix B. The benthic $\delta^{18}O$ contribution from ice volume is calculated by integrating the modelled englacial isotope content over all three modelled ice sheets.

To obtain the deep-water temperature we calculate global temperatures based on CO_2, and we apply a 3000-year running-mean to reflect the lag between the atmosphere and deep-ocean. We then linearly convert deep-water temperatures to deep-water $\delta^{18}O$ contribution.

Results

In this section, we show the results from our 1.5-million-year simulations. First, we present our baseline simulation, after which we explore the mechanisms behind the simulated MPT. In the last section we present experiments with either constant insolation or constant CO_2.

3.1 Baseline results

We conduct the 1.5-million-year baseline simulation, where temperature evolves with prescribed CO_2 from leaf-wax proxy (Yamamoto et al., 2022), caloric summer insolation (Tzedakis et al., 2017), and an albedo feedback. As the leaf-wax record

has higher uncertainties compared to ice-core records, we also conduct the baseline_icecore experiment which is forced by the CO_2 record from Bereiter et al. (2015) instead. However, this continuous CO_2 record covers neither the MPT nor the Early Pleistocene.

170   Fig. 3 shows that the LGM extent is captured by the model. The $\delta^{18}O$ is less depleted where temperatures are high and elevation is low, such as the margins. Fig. 4 shows time-series of the prescribed summer insolation (a), CO_2 (b), the modelled sea level change (c), and benthic $\delta^{18}O$ (d), which are compared to reconstructions by Spratt and Lisiecki et al. (2016) and Ahn et al. (2017). We always add 20% to the modelled sea-level change to approximate ice volume changes in Antarctica, and temperature/density changes of the ocean. This first-order approximation, which is justified by the strong correlation between global climate, Northern Hemisphere ice volume, and Antarctic ice volume (Gomez et al., 2020), but does not account
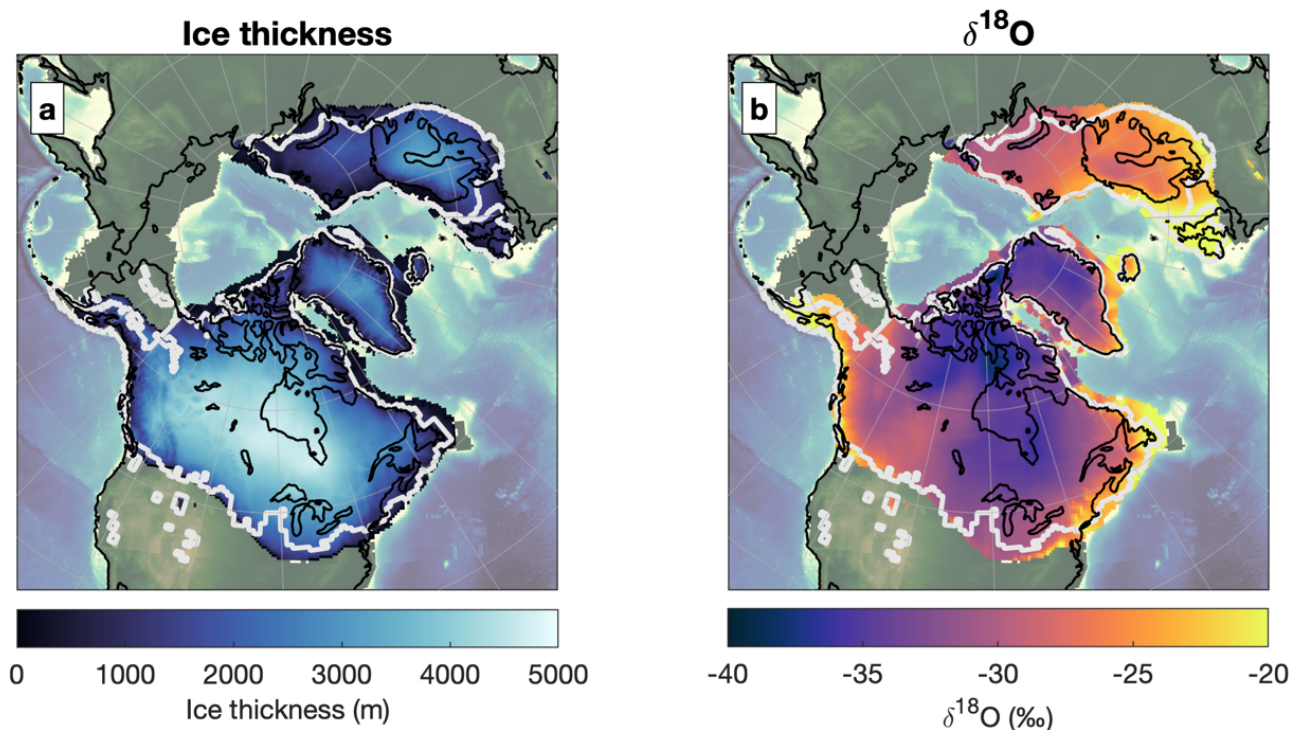
175   for out-of-phase behaviour.

Figure 3. The ice thickness (a), and englacial $\delta^{18}O$ (b) at 20 kyr ago in the baseline simulation. The reconstruction of the extent by Pelter et al. (2015) is shown as white contours. The present-day coastline is shown in black.

      We find that the baseline and baseline_icecore simulations capture most of the glacial-interglacial variability over

180   their time-periods. During their overlapping period, baseline and baseline_icecore match reasonably well. The average absolute difference in ice volume is 13 m.s.l.e. (meters sea level equivalent), reflecting the in-phase characteristics of the two CO_2 records (see Yamamoto et al., 2022).

Peak Northern Hemisphere ice volume during 1500-1000 kyr ago is only a little bit smaller (79±15 m.s.l.e.) compared to the 500-0 kyr ago (98±7 ms.l.e.). Though, at the same time, Early Pleistocene $\delta^{18}O$ levels at glacial maxima are often higher

185   compared to the reconstruction by Ahn et al. (2017). Low benthic $\delta^{18}O$ and high sea-levels cannot be simulated as we do not include Antarctica.

The baseline simulation captures the $\delta^{18}O$ variability of most glacial cycles except for the termination at ~865 kyr (MIS 21), where we simulate partial retreat of the North American ice sheet instead of a full deglaciation. CO_2 is low during the 866 kyr ago insolation peak, but rises while insolation strength decreases. Therefore, insolation compensates the rise in

190   CO_2, preventing a deglaciation. Nevertheless, as our baseline simulations captures the main glacial-interglacial variability during the past 1.5 million years, we can explore the cause behind the MPT in more detail.
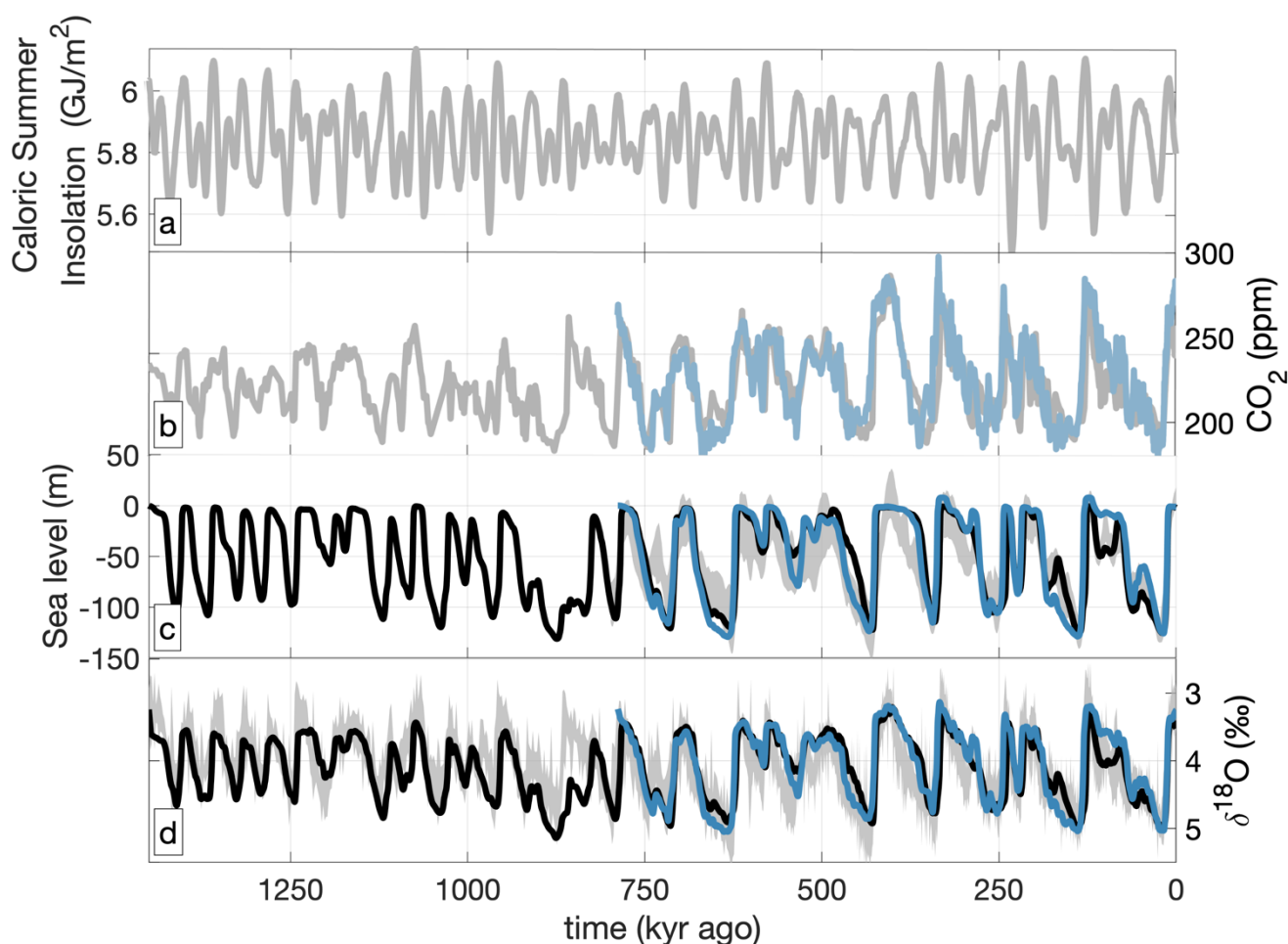
Figure 4. Time-series of caloric summer half-year insolation (a), prescribed CO_2 forcing (b) from ice core (blue; Bereiter et al., 2015) and leaf-wax (grey; Yamamoto et al., 2022). Sea level (c) and benthic $\delta^{18}O$ (d) of the baseline (black) and baseline_ice core (blue) simulations.
195   In grey, the reconstructions of caloric summer half-year insolation by Tzedakis et al., (2017; a), sea level by Spratt and Lisiecki, (2016; c), and $\delta^{18}O$ by Ahn et al. (2017; d).
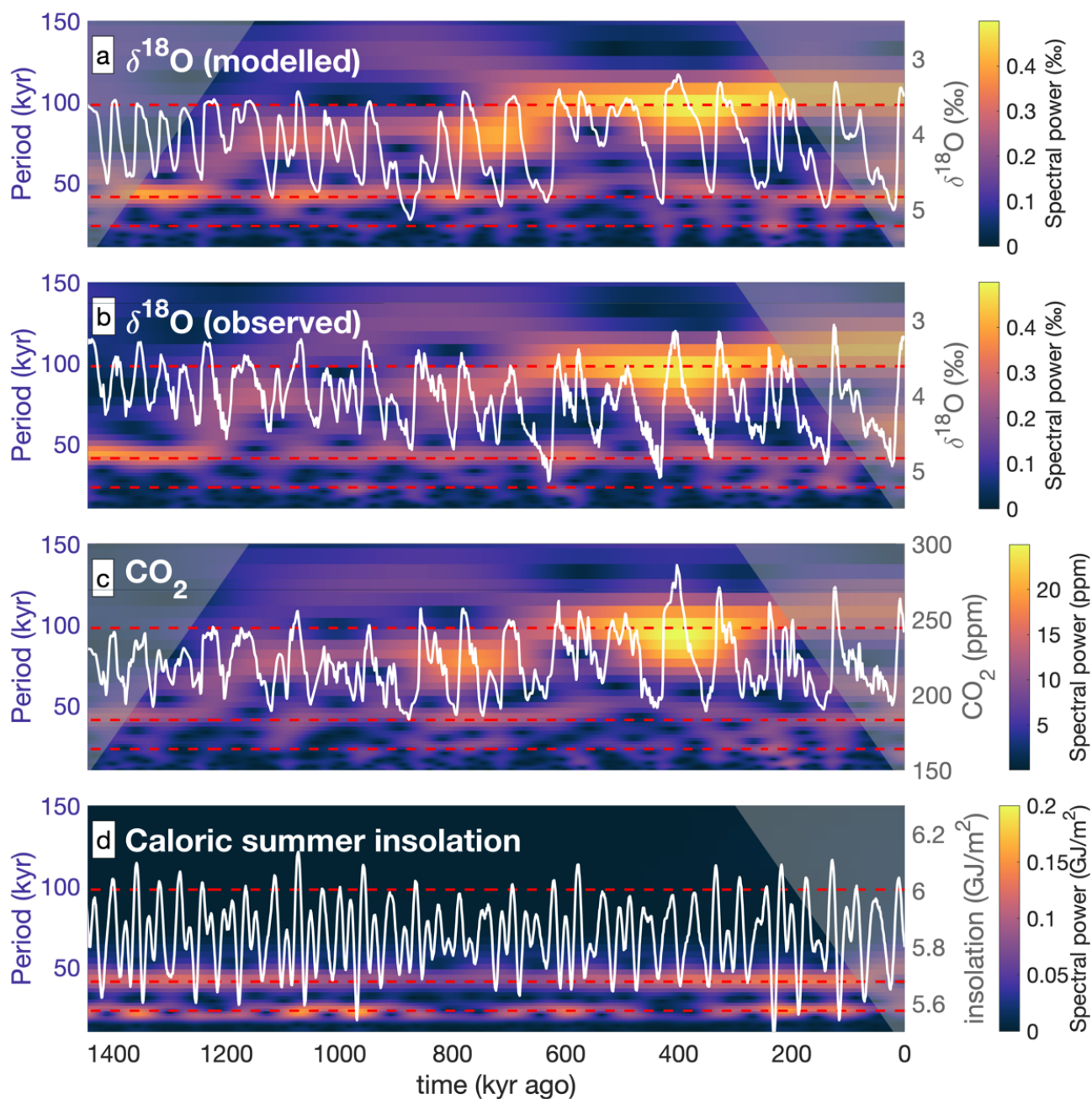
8

Figure 5. Wavelets showing the explained variance and frequency of the modelled δ¹⁸O (a), observed δ¹⁸O (Ahn et al., 2017; b), CO₂ (Yamamoto et al., 2022; c) and caloric summer half-year insolation (Tzedakis et al., 2017; d). Corresponding time-series are shown in white. Red dotted horizontal lines indicate 98 kyr, 41 kyr and 23 kyr periodicities.

3.2 Mechanisms behind the Mid-Pleistocene Transition

In the previous paragraph we showed that we can capture the glacial-interglacial variability in the baseline simulation, without
205 any change in basal friction. In this section we explore the key elements of the frequency change in our baseline simulation.
Fig. 5a shows a wavelet transform of our modelled $\delta^{18}O$ and compares it to the observed record (Fig. 5b). Our simulation
generates the transition from 41-kyr to 100-kyr glacial cycles. The periodicity in the baseline simulation results from the
prescribed insolation and CO_2 forcing, combined with ice sheet feedbacks. There is no change in model-setup or any change
in basal friction. Since the orbital cycles cannot explain the MPT, the main culprit behind our modelled MPT must be the
210 prescribed CO_2 forcing combined with ice-sheet feedback processes.

We can compare the frequency spectrum in the modelled benthic $\delta^{18}O$ to the prescribed caloric summer insolation
and CO_2 that drive the modelled temperature change. Fig 5c and 5d show wavelets of the caloric summer insolation and CO_2
forcing. The caloric summer insolation has a strong ~20 kyr and 41 kyr periodicity, corresponding to precession and obliquity
respectively. The CO_2 forcing has a weak signal in the 41 kyr periodicity, but a strong 100 kyr signal in the Late Pleistocene.
215 This change in frequency takes place when the modelled $\delta^{18}O$ changes from 41 kyr to an average 100 kyr.

These results suggest a regime shift. The 41 kyr periodicity of the Early Pleistocene is generated by the orbital cycles,
as the ice sheet melts during strong summer insolation, which tends to correlate with obliquity maxima. The Late Pleistocene
is more dominated by CO_2, though still paced by the orbital cycles. Terminations take place if both CO_2 and insolation are
high enough, while low CO_2 levels can sometimes cancel the strong summer insolation (e.g., 461 and 175 kyr ago). This would
220 suggest that the MPT could be explained by a decrease of glacial CO_2 levels.

However, when a Late Pleistocene termination does take place, CO_2 levels have continued to decrease. CO_2 levels
rise during terminations, but this rise may be a consequence of the termination rather than the root cause. We did not explicitly
simulate the carbon cycle, and we therefore cannot assess the origins of the CO_2 rise, but we can investigate the feedback
processes leading to the melt of the ice sheets.

225 Fig. 6a shows the ice volume of the North American ice sheet at the onset of all modelled terminations, as a function
of the climate forcing (external forcing index) at that time. The termination onsets are defined as the maxima in the modelled
ice volume that preceded an uninterrupted decrease to (near-) zero ice volume. These onsets therefore represent an integrated
mass balance of around zero and a near-equilibrium with the climate forcing, before the integrated mass balance becomes
negative. This collection of terminations spans an S-shaped curve, indicating a non-linearity between ice sheet volume and
230 climate forcing. If the ice sheet is small (<20 m.s.l.e.) it starts melting at relative warm climates. This changes above the 20
m.s.l.e. threshold and below the 60 m.s.l.e threshold. Within this regime, a small change in the climate forcing will substantially
increase the ice volume threshold for glacial terminations. When exceeding the 60 m threshold, the S-curve gradually levels
off again, and at ice volumes exceeding 75 m.s.l.e., any additional cooling will barely increase the ice volume at terminations.

Moreover, even under LGM-like conditions, these large ice sheets may start to lose mass, which could eventually lead to a
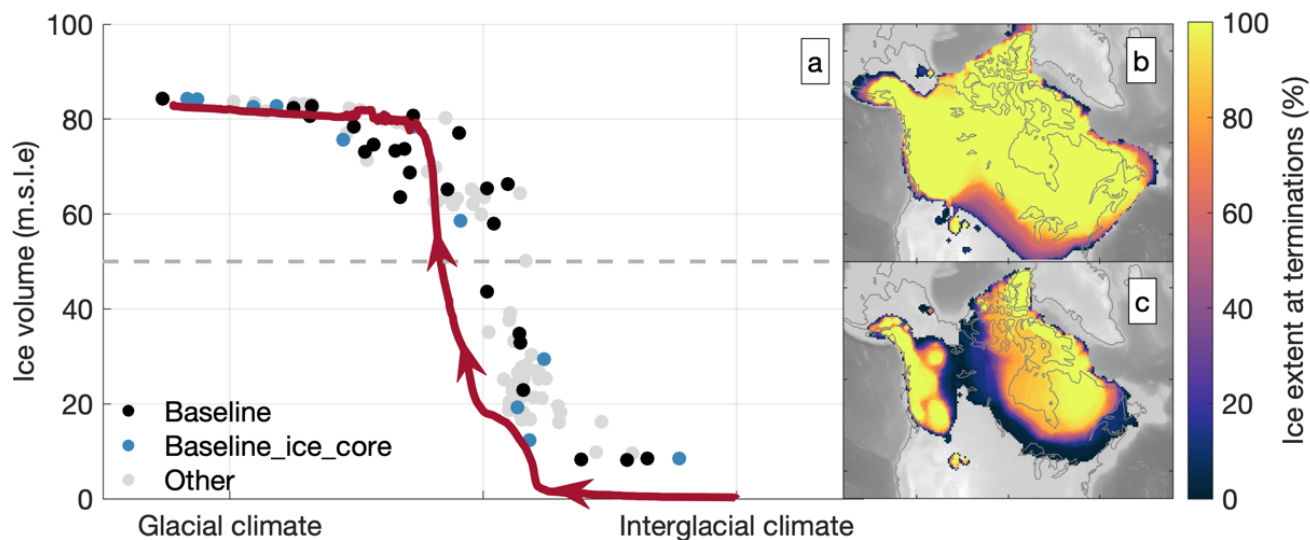235   deglaciation.

Figure 6. Climate forcing (insolation and CO_2) and ice volume at the onset of deglaciations (a). Black circles represent the baseline simulation, whereas blue is the baseline_ice_core. Grey represents the simulations that are introduced in section 3.3 (constant CO_2 or insolation). The red line belongs to the gradual_cooling simulation. The extent of these terminations is shown in panel (b,c), either with ice
240   volumes above (b) or below 50 m.sl.e. (c), with the colours indicating what percentage of the landscape was covered by ice at the start of the termination. We defined a deglaciation as a continuous melt phase leading to an ice volume of less than 8 m.s.l.e.

The nonlinearity between ice volume and climate forcing is further confirmed by the gradual_cooling simulation (see the red line in Fig. 6a), where we altered the climate from interglacial to glacial condition over a period of 1 million years. This simulation provides the ice sheet enough time to readjust to any change in climate forcing, so that it is always (nearly) in
245   equilibrium. As the climate cools, first North-Eastern Canada and the Rocky Mountains will be covered by ice, prompting the first increase in ice volume (<20 m). Afterwards, the majority of growth results from a (high latitude) west-ward expansion of the Laurentide ice sheet, where it has space to grow combined with relatively cold climates. The growth of the ice sheet is largely self-sustained by an increase in ice sheet height and albedo, and if allowed to fully adjust to the climate forcing, creates the near vertical profile seen in Fig. 6a. Eventually, the Laurentide and Cordilleran merge together at an ice volume of 54
250   m.s.l.e, leading to high growth rates due to the merging of ice flows and ablation areas. The strong growth may also explain the "gap" between 40 and 55 m.s.l.e. seen in Fig. 6a. We can see this in Fig. 6b and 6c, where the extent at the onset of every termination event below or above 50 m.s,l.e. are combined. This 50 m.s.l.e. boundary separates most of the separated or merged states of the Cordilerran and Laurentide ice sheets. After the merging, the ice sheet cannot migrate west or north, but is forced to thicken or grow to the warmer south, which eventually slows down the growth and prevents further ice expansion.

255   These results leads to the idea of three regimes of ice-sheet stability: a small ice sheet (<25 m.s.l.e.) which easily melts; a medium ice sheet that can grow rapidly through temperature-elevation feedbacks and the merging of the Cordilleran

11

and Laurentide (>25, < 60 m.s.l.e.); and a large ice sheet (> 60 m.s.l.e.) which is sensitive to a change in climate due to strong positive melt feedbacks, such as the melt-elevation feedback, melt-albedo feedback and the formation of proglacial lakes (see Scherrenberg et al., 2024) and a thermodynamical decoupling (Bintanja and van de Wal, 2008). A sharp increase in CO_2 at

260 glacial terminations could then further accelerate the melt of the ice sheets. A successful termination therefore hinges on whether this melt-feedback loop is triggered. If the ice sheet falls within the large regime, a period with strong summer insolation could more easily trigger the melt feedback loop. CO_2 and insolation conditions for which a small or medium-sized ice sheet could survive, can yield a full collapse of a large ice sheet.

This may also explain why the Late Pleistocene glacial terminations only take place during some, but not all,

265 insolation maxima. Low CO_2 levels may cause an insolation maximum to be skipped if the ice-sheet is medium-sized, but even lower CO_2 concentrations can still generate a full collapse if the ice sheet is large-sized. The periodicity of the benthic $\delta^{18}O$ record is then dominated by the successful terminations, which only occur when the combination of insolation, CO_2 and ice volume is right to trigger a strong enough melt-feedback loop.
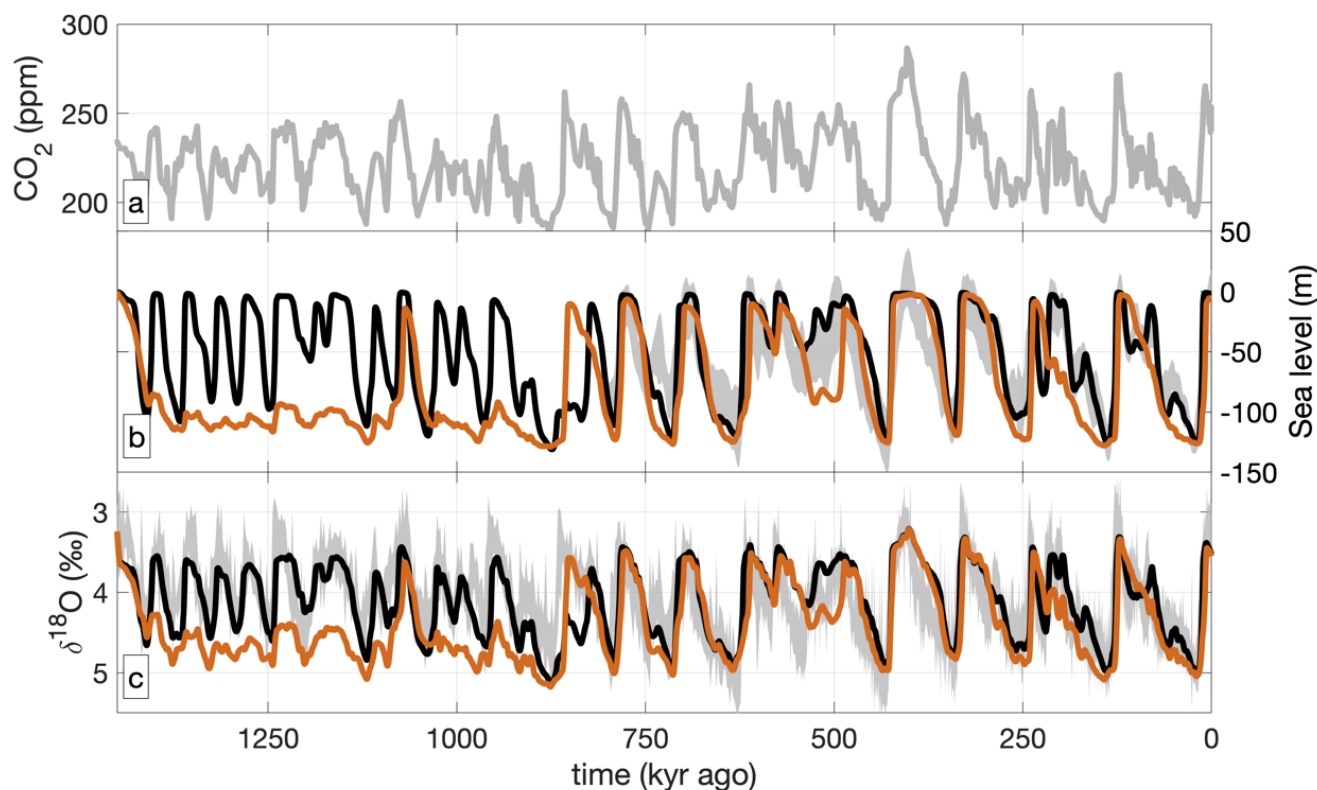
Figure 7. Time-series of prescribed CO_2 (a), sea level (b), $\delta^{18}O$ (c) and of the baseline (black) and constant_insolation (orange) simulations. Reconstructions by Yamamoto et al. (2022; a), Spratt and Lisiecki (2016; b), and Ahn et al (2017; c) are shown in grey.

270

12

3.3 Disentangling CO_2 and insolation

Our baseline simulation can capture the MPT using changes in CO_2 and summer insolation. In this section, we will explore
275 the model response if either one is removed.

In the constant_insolation simulation, we apply the present-day (monthly varying) insolation (implying a constant caloric summer insolation of 5.8 GJ/m^2) to the baseline set-up. In this simulation, temperature change results only from CO_2 and the albedo feedback. Time-series of modelled sea level and benthic $\delta^{18}O$ in the constant_insolation and baseline simulations are shown in Fig. 7. Constant_insolation does not capture the Early Pleistocene glacial cycles, as the relatively
280 low CO_2 levels (~240-250 ppm) fail to initiate a termination in combination with the present-day insolation. The Late-Pleistocene interglacial periods have higher CO_2 levels (>250 ppm), and as such, the terminations are modelled and our simulation has a closer match with reconstructions. This may suggest that the system is more driven by changes in CO_2 during this time. It also indicates that, even if a simulation produces a good match with reconstruction for the last few glacial cycles, there is no guarantee it will do so for the entire Pleistocene.

285 These results indicate that CO_2 alone is not capable of explaining the glacial-interglacial variability of the past 1.5 million years, especially the Early Pleistocene glacial cycles. Therefore, to investigate if orbital cycles alone can capture the MPT, we conduct simulations with constant CO_2 instead.

Fig. 8b shows sea level time-series of simulations forced by constant 240, 220 and 210 ppm CO_2 concentrations (constant_CO2 experiments). The modelled ice volume differs substantially between these three simulations:
290 Constant_CO2_240 yields small ice volumes (generally less than 50 m), which is around half of that in the constant_CO2_220 and constant_CO2_210 simulations. The ice sheet in the constant_CO2_240 simulation mostly melts at 41-kyr intervals. The constant_CO2_220 largely follows the glacial-interglacial periodicity during the Early Pleistocene, and also captures some of the termination events during the Late Pleistocene. Constant_CO2_210 has an even lower CO_2 concentration, leading to long glacial cycles. In all these simulations, the ice sheets can still fully melt, despite these low CO_2 concentrations. This is facilitated
295 by strong positive melt feedbacks and insolation.

Fig. 9 shows wavelet transforms of the sea level and compares it to the summer insolation, which represents the only driver of temperature change in the constant CO_2 simulations. Constant_CO2_240 and constant_CO2_220 simulations show 41-kyr periodicity during the Early Pleistocene, but this persists into the Late-Pleistocene. While constant_CO2_220 and constant_CO2_210 can have increased periodicity when insolation maxima are skipped, neither show a prolonged 100-kyr
300 periodicity. Therefore, the constant_CO2 experiments are almost the reverse of the constant_insolation: Constant CO_2 levels can largely capture the periodicity during the Early Pleistocene glacial cycles, while constant insolation captures the Late Pleistocene instead. These results also suggest that a gradual decrease of glacial CO_2 could prolong glacial periods. With decreasing CO_2 concentrations, fewer insolation maxima lead to terminations, which increases the duration of glacial cycles. A gradual decrease in glacial CO_2 levels could therefore explain the MPT.
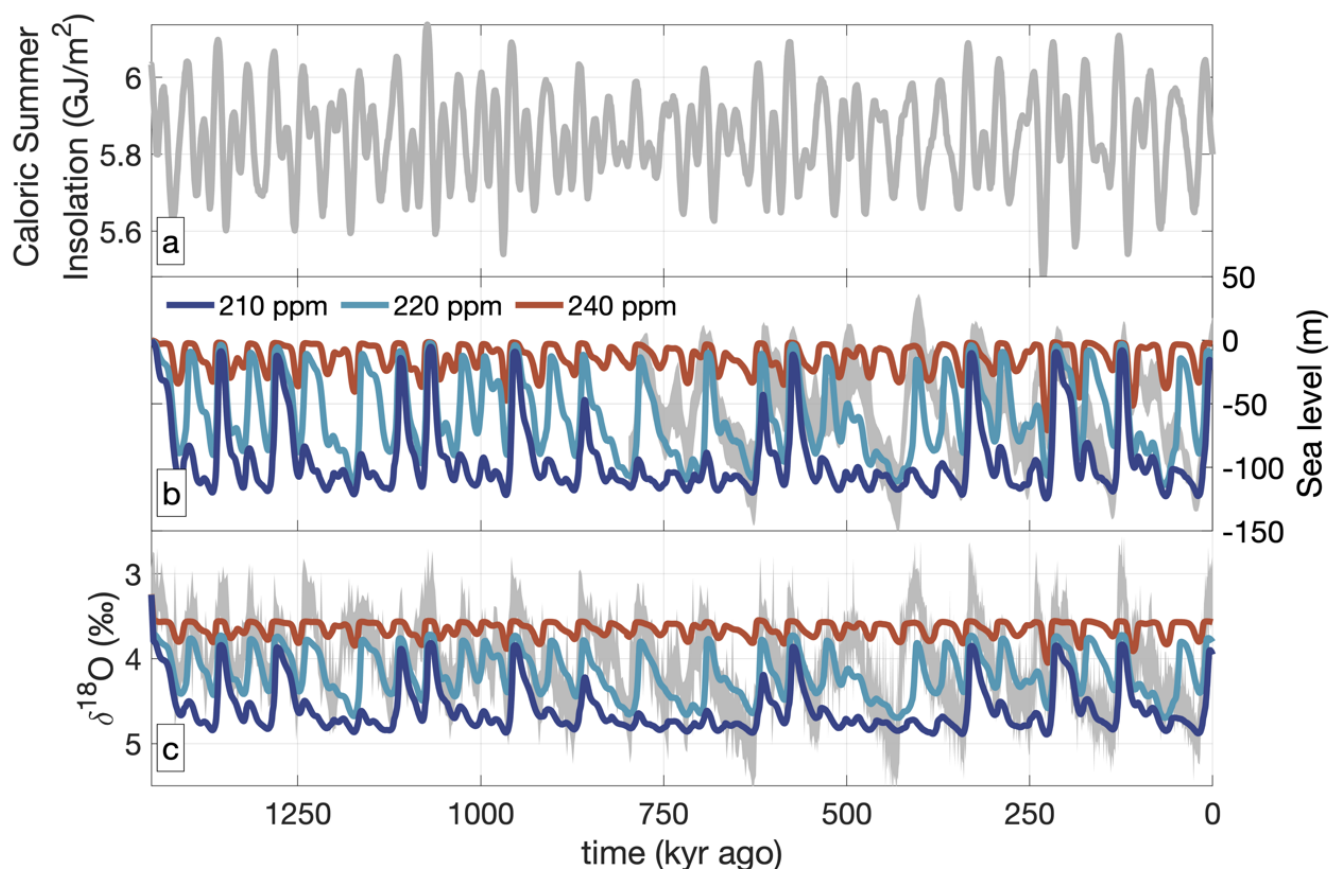
305

13

Figure 8: Time-series of caloric summer half-year insolation (a), sea level (b), and $\delta^{18}O$ (c) of the experiments with constant 240 ppm (red), 220 ppm (cyan) and 210 ppm (blue) CO_2 levels. Observed sea level (Spratt and Lisiecki, 2016; b) and $\delta^{18}O$ (Ahn et al., 2017; c) is shown in grey. Note that the $\delta^{18}O$ of sea water is calculated using CO_2, and all variability of $\delta^{18}O$ in the constant_CO2 simulations therefore results from the ice sheets.

Remarkably, while precession is present in the climate forcing (Fig. 9d), the ~20-kyr signal is mostly absent in the frequency spectrum of the modelled sea level. Terminations are initiated when insolation is strong enough to initiate positive melt feedbacks. The insolation threshold for a termination depends also on CO_2, as the constant_CO2_240, 220 and 210 simulations tend to melt at a caloric summer half-year insolation of roughly 5.9 GJ/m², 6.0 GJ/m² and 6.1 GJ/m² respectively. The terminations tend to occur during peaks in the caloric insolation (generally obliquity), while many smaller peaks (mostly precession) are skipped. Additionally, we have used caloric summer insolation as a driver for temperature change, which accounts for a change in the duration of the melt season that is caused by, and partly compensates the precession signal (see Huybers, 2006). Terminations will therefore tend to correlate to obliquity maxima and filter out precession. This idea, that a threshold in caloric summer insolation can generate precession cancellation, has also been suggested by Tzedakis et al. (2017). Here we find that the feedback processes in the Northern Hemisphere ice sheets (e.g., albedo and topography) can filter out the precession signal. This would also suggest that the glacial cycles of the Early Pleistocene were always paced by all orbital

cycles. However, only the stronger peaks (generally obliquity) in summer insolation can prompt the melt feedback loop, filtering out the weaker insolation maxima (generally precession).
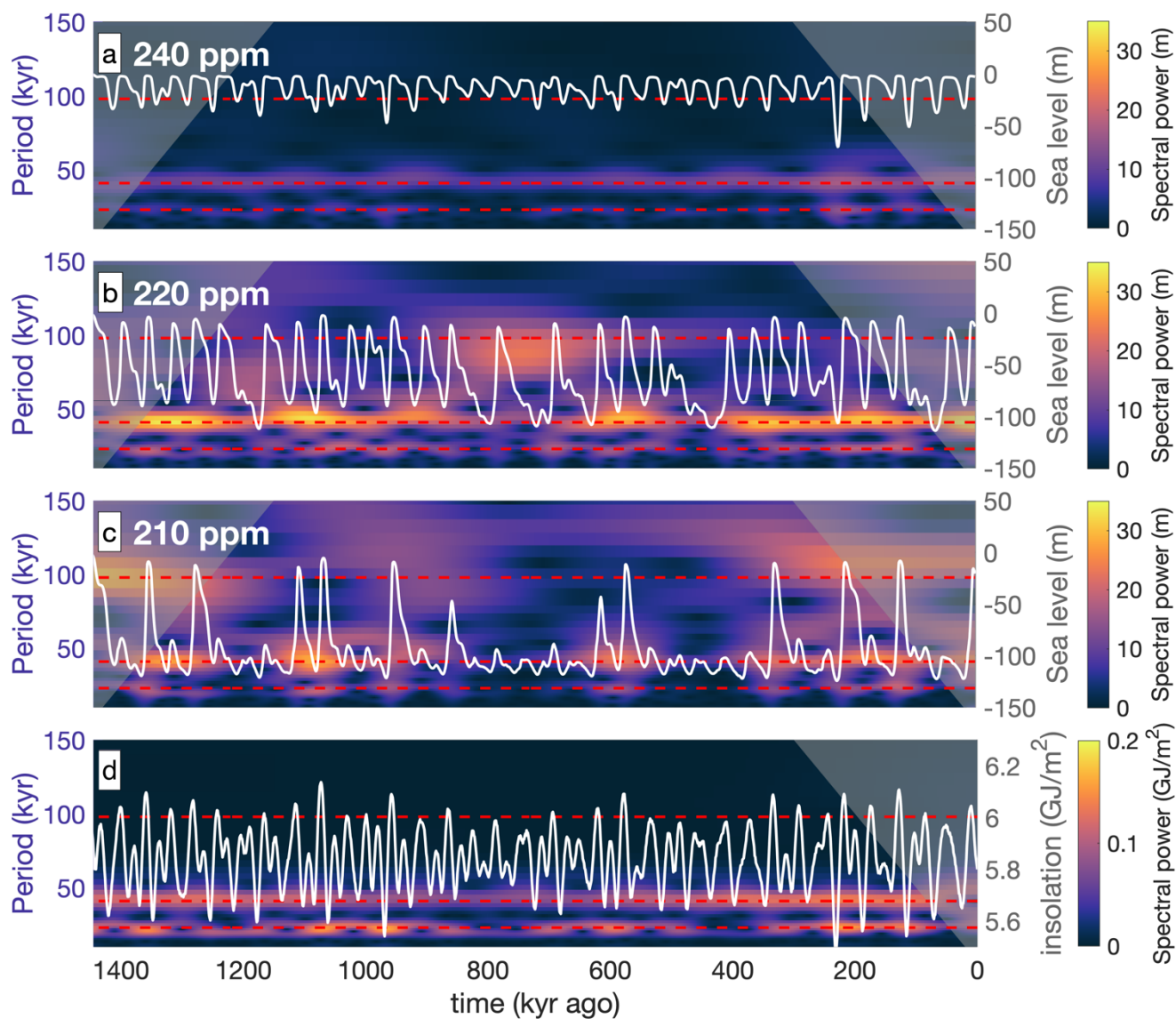
Figure 9. Wavelets showing the frequency in the sea level of 240 ppm (a), 220 ppm (b) and 210 ppm (c), compared to caloric summer half-year insolation (d). Corresponding time-series are shown in white.

325

15

Climate
of the Past
Discussions

Open Access

EGU

4. Discussion

In this study we simulate the Northern Hemisphere ice-sheet evolution during the past 1.5 million years using a climate forcing

330 that depend on prescribed CO_2, insolation and implicit ice-sheet-climate interactions. Using these driving forces, we are able to capture the MPT without any change in model-set-up or basal friction. We find that the modelled MPT results from a change in amplitude and frequency of the CO_2 record. During the Early Pleistocene, CO_2 is high enough to lead to a termination at every obliquity maximum. However, during the Late Pleistocene, CO_2 is too low during some insolation maxima, resulting in a prolongation of the glacial period and thereby increased periodicity. This idea is further confirmed by simulations with

335 constant CO_2 levels, as more insolation maxima are skipped with decreasing CO_2 concentrations.

However, at the end of the Late Pleistocene terminations, CO_2 levels have continued to decrease, but the ice sheets will still melt. We instead propose that the North American ice sheet itself could play a major role in these terminations. In general, as the climate becomes colder, ice sheets can become larger before it starts to attain a negative mass balance. However, we find certain threshold regimes in the North American ice sheet: A small ice sheet will melt at relatively strong CO_2 and

340 insolation. A medium-sized ice sheet grows towards central Canada until eventually, the Laurentide and Cordilleran ice sheets merge. This facilitates a self-sustained growth of the ice sheets, and a small change in the climate forcing will substantially increase the ice volume threshold for glacial terminations. After this merging, we obtain a large-sized ice sheet that has a long margin in the south. This ice sheet is much more sensitive towards insolation increase, and needs low CO_2 and summer insolation to survive. A low glacial CO_2 level can therefore delay a deglaciation of a medium-sized ice sheet, but once the ice

345 sheet is large enough, another insolation maxima may trigger a full termination instead. This is in line with several studies that suggest that the Late Pleistocene terminations only take place if ice volume is large enough (Abe-Ouchi et al., 2013; Parrenin and Paillard, 2003; Bintanja and van de Wal 2008, Berends et al., 2021a). The resulting frequency spectrum of ice volume will then be dominated by the successful terminations, which depend whether a strong melt-feedback loop is triggered. These positive melt feedbacks result from the melt-elevation, melt-albedo feedbacks, and the creation of proglacial lakes. Melt rates

350 are further enhanced by the increase in CO_2 concentrations. Whether these feedbacks are triggered therefore depends on the climate forcing (CO_2 and insolation) as well as the ice volume of the North American ice sheet.

To investigate the relative importance of orbital forcing and CO_2, we conducted simulations with either constant orbital configurations or constant CO_2. If insolation is constant, temperature responds mostly to CO_2, and we can capture the Late Pleistocene terminations, but the Early Pleistocene cycles merge together. If CO_2 levels are constant instead, we can

355 mostly capture the 41-kyr periodicity during the Early Pleistocene, but fail to fully capture the 100-kyr periodicity of the Late Pleistocene cycles. If the constant CO_2 level is low enough, the length of the glacial cycles may increase. We found a very strong sensitivity to CO_2, as a decrease from 240 to 220 ppm CO_2 yields a doubling in ice volume. While it is uncertain if this sensitivity fully holds-up in a fully-coupled Earth-System Model set-up, it does agree with similar experiments using an intermediate complexity model (see Ganopolski and Calov, 2011). However, their 240 ppm CO_2 level already shows some

Climate
of the Past
Discussions

360 skipped terminations at obliquity maxima, while this concentration yielded a persistent 41-kyr periodicity in our simulation instead.

This high sensitivity to CO_2 also highlights the importance of accurate CO_2 reconstructions to detect the changes in long-term CO_2 concentration over the MPT. We have used a leaf-wax CO_2 record (Yamamoto et al., 2022), which has higher uncertainties compared to ice-core records (Bereiter et al., 2015). These CO_2 records match well during their overlapping

365 period and both are capable of reproducing the glacial-interglacial variability. Although, the CO_2 levels before 800-kyr ago is still uncertain as continuous ice-core records do not cover this period yet. Nevertheless, the shift from 41 to 100 kyr periodicity in the CO_2 record is also found in boron-based CO_2 reconstructions (e.g., Dyez et al., 2018), indicating that this frequency shift in CO_2 is consistent among different CO_2 records. Additionally, both Yamamoto et al. (2022) and Hönisch et al. (2009) find a decrease in glacial CO_2 concentrations across the MPT. Our results also agree with Watanabe et al. (2023), who found based

370 on ice-sheet model simulations that the Early Pleistocene glacial cycles follow from orbital oscillations, with minimal effect from CO_2.

In order to simulate 1.5 million years requires a trade-off between explicitly modelling processes and computational time. While we simulate some ice-sheet climate interactions, they are more complex in reality. For example, we do not include any feedback from the ocean circulation or sea ice. Another limitation of our approach is that the climate forcing is only based

375 on just two ensemble-mean climate time-slices. This choice was made due to the large differences between climate models, whereas the PMIP4 ensemble shows good results (see Kageyama et al., 2021). These GCM simulations were conducted with a prescribed LGM ice sheet, and the high albedo of the ice sheet leaves a cold imprint on the temperature field and creates a large temperature gradient between ice and ice-free areas. If the ice volume is close to LGM, the extent will therefore be close as well. We do not see this as a limitation, as our main goal here is not to make accurate reconstructions, but rather focus on

380 the long-term ice volume change and the processes behind the change in glacial cycle periodicity.

The simulated MPT, and much of the glacial-interglacial variability of the past 1.5 million years results from a change in the prescribed CO_2 forcing, but the origin of the amplitude and frequency in the CO_2 record remains uncertain and was not studied here. As we use prescribed CO_2, (failed) terminations are already present in the CO_2 record: High CO_2 levels could be a symptom of successful terminations, while low CO_2 levels could be a symptom of unsuccessful terminations. Our model

385 then replicates these failed and successful terminations. However, even with constant CO_2 levels, we can simulate many terminations during the Late Pleistocene, even though the overall periodicity does not match. A low constant CO_2 concentration (210 ppm) does skip several of these terminations. This suggest that the melt of the ice sheet could have been prompted by insolation, but it has been enhanced by an increase in CO_2. However, our simulations do not explain the decrease in glacial CO_2 concentrations, which could of course be related to ice-sheet-carbon-cycle interactions. Therefore, while our results

390 suggest that CO_2 can have a key role in the MPT, and that a decrease in glacial CO_2 could lengthen glacial cycles, to truly uncover the origin of the MPT will require a coupled ice-sheet-climate-carbon-cycle model.

Appendix A: Climate forcing

The ice-sheet is forced with transient changing precipitation and temperature forcing. To reduce computational resources
395   compared to coupled ice-climate set-ups, we interpolate between pre-calculated LGM and PI climates using a matrix method
(see Berends et al., 2018; Scherrenberg et al., 2023). For the monthly ($mnth$) temperature forcing (T) at each grid-cell (x, y),
we use the following linear interpolation:

$$T(x, y, mnth) = w_T(x, y)\, T_{PI}(x, y, mnth) + \left(1 - w_T(x, y)\right) T_{LGM}(x, y, mnth). \tag{A1}$$

w_T represents the interpolation weight and depends on external forcing (w_e) and an albedo feedback (w_a). We allow some
400   extrapolation for colder than LGM or warmer than present-day climates, though each interpolation weight is capped between
-0.5 and 1.5.

      The external forcing interpolation weight depends on CO_2 ($CO2$; obtained from Yamamoto et al., 2022 or Bereiter et
al., 2015) and caloric summer half-year insolation at 65°N ($Q_{65°N}$; Tzedakis et al., 2017). We use the following equation to
calculate the weight from the prescribed forcing:

405
$$w_e = \frac{CO2 - 190\ \text{ppm}}{280\ \text{ppm} - 190\ \text{ppm}} + \frac{Q_{65°N} - 5.8\ GJ/m^2}{0.55\ GJ/m^2}. \tag{A2}$$

This ratio was obtained by conducting a preliminary experiment based on de Boer et al. (2013) and Berends et al. (2021b),
where we modify w_e to obtain good agreement with benthic $\delta^{18}O$ from Ahn et al., (2017). We then fitted the resulting w_e to
CO_2 and insolation and fine-tuned it to obtain Eq. (A2).

      To calculate w_a (the albedo feedback), we first calculate 2D fields of the amount of insolation that is absorbed by the
410   surface (I). This depends on surface albedo (α_s) and the grid-cells insolation at the top of the atmosphere (Q):

$$I(x, y) = \sum_{m=1}^{12} Q(x, y, mnth) \left(1 - \alpha_s(x, y, mnth)\right). \tag{A3}$$

The albedo is generated by the ice-sheet model. First a background albedo is applied based on the ice (0.5), land (0.2) and
ocean (0.1) surfaces. We then add a layer of snow that can increase albedo to up to 0.85. Using masks, climate and insolation
from PI and LGM, we calculate absorbed insolation fields for the climate time-slices as well (I_{PI} and I_{LGM}). Using these three
415   fields, we calculate a local interpolation weight for absorbed insolation (w_i):

$$w_i(x, y) = \left(I(x, y) - I_{LGM}(x, y)\right) / \left(I_{PI}(x, y) - I_{LGM}(x, y)\right). \tag{A4}$$

Albedo has both a local and regional effect. We apply a gaussian smoothing of 200 km on w_i to obtain $w_{i,smooth}$. We also
calculate a domain-average w_i, which is $w_{i,domain}$. These three interpolation fields are then combined to obtain the albedo
feedback, following the approach by Berends et al. (2018):

$$w_a(x, y) = \frac{w_i(x, y) + 3\, w_{i,smooth}(x, y) + 3\, w_{i,domain}(x, y)}{7}. \tag{A5}$$

420
        .

The albedo interpolation weight is then combined with the external forcing to obtain the w_T from Eq. (A1):

Climate
of the Past
Discussions

$$w_T(x,y) = \frac{3\,w_e(x,y) + w_a(x,y)}{4}.$$ (A6)

425 As such, temperature depends on CO_2, caloric summer half-year insolation and a spatially varying albedo/insolation field.

To interpolate precipitation (P), we use the following equation:

$$P = exp\left(\begin{array}{l}(1 - w_P(x,y))\log(P_{PI}(x,y,mnth)) \\ + w_P(x,y)\log(P_{LGM}(x,y,mnth))\end{array}\right).$$ (A7)

w_P is the interpolation weight for precipitation, and is calculated with respect to local and domain-wide topography changes, reflecting changes in atmospheric circulation and the dry climates on top of ice domes. First, we calculate the total change in 430 topography (s) in the domain with respect to PI and LGM:

$$w_{s,domain} = \frac{\sum s - \sum s_{PI}}{\sum s_{LGM} - \sum s_{PI}}$$ (A8)

$w_{s,domain}$ is the interpolation weight from a domain-wide change in topography. If a grid-cell has ice during the LGM, and thus a large change in topography, we also interpolate with the local topography change:

$$w_{s,local}(x,y) = \frac{S(x,y) - S_{PI}(x,y)}{S_{LGM}(x,y) - S_{PI}(x,y)}\,w_{s,domain}(x,y).$$ (A9)

435 However, if a grid cell had ice during neither PI nor LGM, $w_{s,local}$ is equal to $w_{s,domain}$. To obtain the final interpolation weight (w_P), we combine the local and domain-wide topography change:

$$w_P(x,y) = w_{s,local}(x,y)\,w_{s,domain}(x,y).$$ (A10)

Appendix B: $\delta^{18}O$ model

IMAU-ICE includes a benthic $\delta^{18}O$ routine, which calculates the $\delta^{18}O$ contribution from ice volume and deep-water 440 temperature. This method is based on de Boer et al. (2013) and Berends et al. (2021b). Deep water temperature change (ΔTd) is based on CO_2 levels ($CO2$):

$$\Delta Td = \left(\frac{280\text{ ppm} - CO2}{280\text{ ppm} - 190\text{ ppm}}\right)2.5°C \qquad .$$ (B1)

A 3000 kyr running-mean is applied to reflect the lag between atmospheric and deep-ocean temperatures. We then multiply this by 0.28 to obtain the $\delta^{18}O$ contribution from deep-water temperature.

445 For the ice sheets, we calculate a $\delta^{18}O$ contribution for every grid-cell (I). We calculate a $\delta^{18}O$ of snow accumulation based on Clarke et al. (2005):

$$I(x,y) = I_{ref}(x,y) + 0.35(T(x,y) - T_{PI}(x,y) - \gamma(s(x,y) - s_{PI}(x,y)) - 0.0062(s(x,y) - s_{PI}(x,y)).$$ (B2)

Here, T represents the annual mean temperature, and s represents the surface topography. The total contribution from each ice-sheet is added together and multiplied by 1.1 to reflect that we do not simulate Antarctica. I_{ref}, which is the (present-day) 450 reference isotope concentrations, is calculated using the following parameterization by Zwally and Giovinetto (1997):

$$I_{ref}(x,y) = 0.691 * T(x,y) - 202.172. \tag{B3}$$

We then add the deep-water and ice-sheet contributions together to obtain the benthic $\delta^{18}O$.

Code availability: The ice-sheet model IMAU-ICE is described by Berends et al. (2022). The model version used in this study,
455   as well as configuration files are available on Zenodo [DOI will be added upon acceptation]. To conduct the simulations,
additional files are required. These include the prescribed CO_2 (see Bereiter et al., 2015 and Yamamoto et al., 2022), climate
forcing (PMIP4 database: https://esgf-node.ipsl.upmc.fr/search/cmip6-ipsl/, last access: 16 Aug 2024), insolation (Laskar et
al., 2004, Tzedakis et al., 2017), initial topography (ETOPO: https://doi.org/10.7289/V5C8276M, Amante and Eakins, 2009;
BedMachine: https://doi.org/10.5067/5XKQD5Y5V3VN, NSIDC, 2024), and basal friction (Gowan et al., 2019 and Laske
460   and Masters, 1997). For more information, contact the corresponding author.

Data availability: The results are available in a 2 kyr (2D fields) and 100-year (scalar) output frequency at Zenodo [DOI will
be added upon acceptation]. Additional 2D fields can be requested by contacting the corresponding author.

465   *Author contributions.* MS conducted the simulations and has written the manuscript. The set-up for the experiments was
created by RW, CB and MS. CB provided model support. All authors have provided input to the manuscript and analysis of
the results.

Competing interest. The authors declare that they have no conflict of interest.
470

References

Abe-Ouchi, A., Saito, F., Kawamura, K., Raymo, M. E., Okuno, J., Takahashi, K., and Blatter, H.: Insolation-driven 100,000-
480   year glacial cycles and hysteresis of ice-sheet volume, Nature, 500, 190–193, https://doi.org/10.1038/nature12374, 2013.
Adkins, J. F.: The role of deep ocean circulation in setting glacial climates, Paleoceanography, 28, 539–561,
https://doi.org/10.1002/palo.20046, 2013.

Ahn, S., Khider, D., Lisiecki, L. E., and Lawrence, C. E.: A probabilistic Pliocene–Pleistocene stack of benthic δ18O using a profile hidden Markov model, Dynam. Stat. Clim. Syst., 2, dzx002, https://doi.org/10.1093/climsys/dzx002, 2017.

485 Alder, J. R. and Hostetler, S. W.: Applying the Community Ice Sheet Model to evaluate PMIP3 LGM climatologies over the North American ice sheets, Clim. Dynam., 53, 2807–2824, https://doi.org/10.1007/s00382-019-04663-x, 2019.

Amante, C. and Eakins, B. W.: ETOPO1 1 Arc-Minute Global Relief Model: Procedures, Data Sources and Analysis. NOAA Technical Memorandum NESDIS NGDC-24, National Geophysical Data Center, NOAA [dataset], https://doi.org/10.7289/V5C8276M, 2009.

490 Bereiter, B., Eggleston, S., Schmitt, J., Nehrbass-Ahles, C., Stocker, T. F., Fischer, H., Kipfstuhl, S., and Chappellaz, J.: Revision of the EPICA Dome C CO2 record from 800 to 600kyr before present, Geophys. Res. Lett., 42, 542–549, https://doi.org/10.1002/2014GL061957, 2015.

Berends, C. J., de Boer, B., and van de Wal, R. S. W.: Application of HadCM3@Bristolv1.0 simulations of paleoclimate as forcing for an ice-sheet model, ANICE2.1: set-up and benchmark experiments, Geosci. Model Dev., 11, 4657–4675,
495 https://doi.org/10.5194/gmd-11-4657-2018, 2018.

Berends, C. J., Köhler, P., Lourens, L. J., and van de Wal, R. S. W.: On the cause of the mid-Pleistocene transition, Rev. Geophys., 59, e2020RG000727, https://doi.org/10.1029/2020RG000727, 2021a.

Berends, C. J., de Boer, B., and van de Wal, R. S. W.: Reconstructing the evolution of ice sheets, sea level, and atmospheric CO2 during the past 3.6 million years, Clim. Past, 17, 361–377, https://doi.org/10.5194/cp-17-361-2021, 2021b.

500 Berends, C. J., Goelzer, H., Reerink, T. J., Stap, L. B., and van de Wal, R. S. W.: Benchmarking the vertically integrated ice-sheet model IMAU-ICE (version 2.0), Geosci. Model Dev., 15, 5667– 5688, https://doi.org/10.5194/gmd-15-5667-2022, 2022.

Bintanja, R., van de Wal, R. S. W., and Oerlemans, J.: Global ice volume variations through the last glacial cycle simulated by a 3-D ice dynamical model, Quatern. Int., 95–96, 11–23, 2002.

505 Bintanja, R. and van de Wal, R. S. W.: North American ice-sheet dynamics and the onset of 100,000-year glacial cycles, Nature, 454, 869–872, https://doi.org/10.1038/nature07158, 2008.

Blackburn, T., Kodama, S., and Piccione, G.: Eccentricity paces late Pleistocene glaciations. Geophysical Research Letters, 51, e2024GL108751. https://doi.org/10.1029/2024GL108751, 2024.

Bouttes, N., Roche, D. M., and Paillard, D.: Impact of strong deep ocean stratification on the glacial carbon cycle,
510 Paleoceanography, 24, Artn Pa3203 https://doi.org/10.1029/2008pa001707, 2009.

Brovkin, V., Ganopolski, A., Archer, D., Munhoven, G.: Glacial CO2 cycle as a succession of key physical and biogeochemical processes. Clim. Past 8, 251–264. https://doi.org/10.5194/cp-8-251-2012, 2012.

Bueler, E. and Brown, J.: The shallow shelf approximation as a sliding law in a thermomechanically coupled ice sheet model, J. Geophys. Res., 114, F03008, https://doi.org/10.1029/2008JF001179, 2009.

515 Chalk, T. B., Hain, M. P., Foster, G. L., Rohling, E. J., Sexton, P. F., Badger, M. P. S., Cherry, S. G., Hasenfratz, A. P., Haug, G. H., Jaccard, S. L., Martínez-García, A., Palike, H., Pancost, R. D., and Wilson, P. A.: Causes of ice age intensification

across the Mid-Pleistocene Transition, P. Natl. Acad. Sci. USA, 114, 13114–13119, https://doi.org/10.1073/pnas.1702143114, 2017.

Clark, P. U. and Pollard, D.: Origin of the Middle Pleistocene Transition by ice sheet erosion of regolith, Paleoceanography,
520   13, 1–9, https://doi.org/10.1029/97PA02660, 1998.

Clarke, G. K. C., Lhomme, N., and Marshall, S. J.: Tracer transport in the Greenland Ice Sheet – three-dimensional isotopic stratigraphy, Quaternary Sci. Rev. 24, 155–171. https://doi.org/10.1016/j.quascirev.2004.08.021, 2005.

Da, J., Zhang, Y. G., Li, G., Meng, X., Ji, J.: Low CO_2 levels of the entire Pleistocene epoch. Nat. Commun. 10, 1e9. https://doi.org/10.1038/s41467-019-12357-5, 2019.

525   de Boer, B., van de Wal, R. S. W., Lourens, L. J., Bintanja, R., and Reerink, T. J.: A continuous simulation of global ice volume over the past 1 million years with 3-D ice-sheet models, Clim. Dynam., 41, 1365–1384, 2013.

Detlef, H., Belt, S. T., Sosdian, S. M., Smik, L., Lear, C. H., Hall, I. R., Cabedo-Sanz, P., Husum, K., and Kender, S.: Sea ice dynamics across the Mid-Pleistocene transition in the Bering Sea, Nat. Commun., 9, 941, https://doi.org/10.1038/s41467-018-02845-5, 2018.

530   Dyez, K. A., Hönisch, B., and Schmidt, G. A.: Early Pleistocene Obliquity-Scale pCO2 Variability at ~1.5 Milion Years Ago, Paleoceanography and Paleoclimatology, 33, 1270–1291, https://doi.org/10.1029/2018PA003349, 2018.

Farmer, J. R., Honisch, B., Haynes, L. L., Kroon, D., Jung, S., Ford, H. L., Raymo, M. E., Jaume-Segui, M., Bell, D. B., Goldstein, S. L., Pena, L. D., Yehudai, M., and Kim, J.: Deep Atlantic Ocean carbon storage and the rise of 100,000-year glacial cycles, Nat. Geosci., 12, 355–360, https://doi.org/10.1038/s41561-019-0334-6, 2019.

535   Feldmann, J., Albrecht, T., Khroulev, C., Pattyn, F., and Levermann, A.: Resolution-dependent performance of grounding line motion in a shallow model compared to a full-Stokes model according to the MISMIP3d intercomparison, J. Glaciol., 60, 353–360, https://doi.org/10.3189/2014JoG13J093, 2014.

Feng, F. and Bailer-Jones, C. A. L.: Obliquity and precession as pacemakers of Pleistocene deglaciations. Quat. Sci. Rev. 122, 166e179, https://doi.org/10.1016/ j.quascirev.2015.05.006, 2015.

540   Fettweis, X., Hofer, S., Krebs-Kanzow, U., Amory, C., Aoki, T., Berends, C. J., Born, A., Box, J. E., Delhasse, A., Fujita, K., Gierz, P., Goelzer, H., Hanna, E., Hashimoto, A., Huybrechts, P., Kapsch, M.-L., King, M. D., Kittel, C., Lang, C., Langen, P. L., Lenaerts, J. T. M., Liston, G. E., Lohmann, G., Mernild, S. H., Mikolajewicz, U., Modali, K., Mottram, R. H., Niwano, M., Noël, B. P. Y., Ryan, J. C., Smith, A., Streffing, J., Tedesco, M., van de Berg, W. J., van den Broeke, M. R., van de Wal, R. S. W., van Kampenhout, L., Wilton, D., Wouters, B., Ziemen, F., and Zolles, T.: GrSMBMIP: intercomparison of the
545   modelled 1980-2012 surface mass balance over the Greenland Ice Sheet, The Cryosphere 14, 3935-3958, https://doi.org/10.5194/tc-14-3935-2020, 2020.

Ganopolski, A. and Calov, R.: The role of orbital forcing, carbon dioxide and regolith in 100 kyr glacial cycles, Clim. Past, 7, 1415–1425, https://doi.org/10.5194/cp-7-1415-2011, 2011.

Gomez, N., Gregoire, L., Mitrovica, J., and Payne, A.: Laurentide-Cordilleran Ice Sheet saddle collapse as a contribution to
550   meltwater pulse 1A, Geophys. Res. Lett., 42, 3954–3962, https://doi.org/10.1002/2015GL063960, 2015.

Gowan, E. J., Niu, L., Knorr, G., and Lohmann, G.: Geology datasets in North America, Greenland and surrounding areas for use with ice sheet models, Earth Syst. Sci. Data, 11, 375–391, https://doi.org/10.5194/essd-11-375-2019, 2019.

Hasenfratz, A. P., Jaccard, S. L., Martínez-García, A., Sigman, D. M., Hodell, D. A., Vance, D., Bernasconi, S. M., Kleiven, H. F., Haumann, F. A., and Haug, G. H.: The residence time of Southern Ocean surface waters and the 100 000-year ice age cycle, Science, 363, 1080–1084, https://doi.org/10.1126/science.aat7067, 2019.

Hinck, S., Gowan, E. J., Zhang, X., and Lohmann, G.: PISM-LakeCC: Implementing an adaptive proglacial lake boundary in an ice sheet model, The Cryosphere, 16, 941–965, https://doi.org/10.5194/tc-16-941-2022, 2022.

Hobart, B., Lisiecki, L. E., Rand, D., Lee, T., and Lawrence, C. E.: Late Pleistocene 100-kyr glacial cycles paced by precession forcing of summer insolation, Nat. Geosci., 16, 717–722, https://doi.org/10.1038/s41561-023-01235-x, 2023.

Hönisch, B., Hemming, N.G., Archer, D., Siddall, M., McManus, J.F.: Atmospheric carbon dioxide concentration across the mid-Pleistocene transition. Science 324, 1551–1554, https://doi.org/10.1126/science.1171477, 2009.

Huybers, P. and Wunsch, C.: Obliquity pacing of the late Pleistocene glacial terminations, Nature, 434, 491–494, 2005.

Huybers, P.: Early Pleistocene glacial cycles and the integrated summer insolation forcing, Science, 313, 508–511, https://doi.org/10.1126/science.1125249, 2006.

Huybers, P. and Tziperman, E.: Integrated summer insolation forcing and 40,000-year glacial cycles: The perspective from an ice-sheet/energy-balance model, Paleoceanography, 23, https://doi.org/10.1029/2007PA001463, 2008.

Huybers, P.: Combined obliquity and precession pacing of late Pleistocene deglaciations, Nature, 480, 229–232, https://doi.org/10.1038/nature10626, 2011.

Huybrechts, P. and de Wolde, J.: The dynamic response of the Greenland and Antarctic ice sheets to multiple-century climatic warming, J. Climate 1, 2169–2188, 1999.

Kageyama, M., Albani, S., Braconnot, P., Harrison, S. P., Hopcroft, P. O., Ivanovic, R. F., Lambert, F., Marti, O., Peltier, W. R., Peterschmitt, J.-Y., Roche, D. M., Tarasov, L., Zhang, X., Brady, E. C., Haywood, A. M., LeGrande, A. N., Lunt, D. J., Mahowald, N. M., Mikolajewicz, U., Nisancioglu, K. H., Otto-Bliesner, B. L., Renssen, H., Tomas, R. A., Zhang, Q., Abe-Ouchi, A., Bartlein, P. J., Cao, J., Li, Q., Lohmann, G., Ohgaito, R., Shi, X., Volodin, E., Yoshida, K., Zhang, X., Zheng, W.: The PMIP4 contribution to CMIP6 – Part 4: Scientific objectives and experimental design of the PMIP4-CMIP6 Last Glacial Maximum experiments and PMIP4 sensitivity experiments, Geosci. Model Dev., 10, 4035–4055, https://doi.org/10.5194/gmd-10-4035-2017, 2017.

Kageyama, M., Braconnot, P., Harrison, S. P., Haywood, A. M., Jungclaus, J. H., Otto-Bliesner, B. L., Peterschmitt, J.-Y., Abe- Ouchi, A., Albani, S., Bartlein, P. J., Brierley, C., Crucifix, M., Dolan, A., Fernandez-Donado, L., Fischer, H., Hopcroft, P. O., Ivanovic, R. F., Lambert, F., Lunt, D. J., Mahowald, N. M., Peltier, W. R., Phipps, S. J., Roche, D. M., Schmidt, G. A., Tarasov, L., Valdes, P. J., Zhang, Q., Zhou, T.: The PMIP4 contribution to CMIP6 – Part 1: Overview and overarching analysis plan, Geosci. Model Dev. 11, 1033–1057, https://doi.org/10.5194/gmd-11-1033-2018, 2018

Kageyama, M., Harrison, S. P., Kapsch, M.-L., Löfverström, M., Lora, J. M., Mikolajewicz, U., Sherriff-Tadano, S., Vadsaria, T., Abe-Ouchi, A., Bouttes, N., Chandan, D., Gregoire, L. J., Ivanovic, R. F., Izumi, K., LeGrande, A. N., Lhardy, F.,

585   Lohmann, G., Morozova, P. A., Ohgaito, R., Paul, A., Peltier, W. R., Poulsen, C. J., Quiquet, A., Roche, D. M., Shi, X.,
        Tierney, J. E., Valdes, P. J., Volodin, E., and Zhu, J.: The PMIP4 Last Glacial Maximum experiments: preliminary results
        and comparison with the PMIP3 simulations, Clim. Past, 17, 1065–1089, https://doi.org/10.5194/cp-17-1065-2021, 2021.

       Köhler, P. and Bintanja, R.: The carbon cycle during the Mid Pleistocene Transition: the Southern Ocean Decoupling
        Hypothesis, Clim. Past, 4, 311–332, https://doi.org/10.5194/cp-4-311-2008, 2008.

590   Kurahashi-Nakamura, T., Abe-Ouchi, A., and Yamanaka, Y.: Effects of physical changes in the ocean on the atmospheric
        pCO_2: glacial-interglacial cycles, Clim. Dynam., 35, 713–719, https://doi.org/10.1007/s00382-009-0609-5, 2010.

       Laskar, J., Robutel, P., Joutel, F., Gastineau, M., Correia, A. C. M., and Levrard, B.: A long-term numerical solution for the
        insolation quantities of the Earth, Astron. Astrophys., 428, 261–285, https://doi.org/10.1051/0004-6361:20041335, 2004.

       Laske, G. and Masters, G.: A Global Digital Map of Sediment Thickness, EOS T. Am. Geophys. Un., 78, F483, 1997.

595   Lear, C. H., Billups, K., Rickaby, R. E. M., Diester-Haass, L., Mawbey, E. M., and Sosdian, S. M.: Breathing more deeply:
        Deep   ocean   carbon   storage   during   the   mid-Pleistocene   climate   transition,   Geology,   44,   1035–1038,
        https://doi.org/10.1130/G38636.1, 2016.

       Leguy, G. R., Lipscomb, W. H., and Asay-Davis, X. S.: Marine ice sheet experiments with the Community Ice Sheet Model,
        The Cryosphere, 15, 3229–3253, https://doi.org/10.5194/tc-15-3229- 2021, 2021.

600   Le Meur, E. and Huybrechts, P.: A comparison of different ways of dealing with isostasy: examples from modeling the
        Antarctic ice sheet during the last glacial cycle, Ann. Glaciol., 23, 309–317, https://doi.org/10.3189/S0260305500013586,
        1996.

       Lisiecki, L. E.: Links between eccentricity forcing and the 100,000-year glacial cycle, Nat. Geosci., 3, 349–352,
        https://doi.org/10.1038/ngeo828, 2010.

605   Martin,   J.   H.:   Glacial-interglacial CO_2 change: the   iron   hypothesis,   Paleoceanography,   5,   1–13,
        https://doi.org/10.1029/PA005i001p00001, 1990.

       Martin, M. A., Winkelmann, R., Haseloff, M., Albrecht, T., Bueler, E., Khroulev, C., and Levermann, A.: The Potsdam Parallel
        Ice Sheet Model (PISM-PIK) – Part 2: Dynamic equilibrium simulation of the Antarctic ice sheet, The Cryosphere, 5, 727–
        740, https://doi.org/10.5194/tc-5-727-2011, 2011.

610   Martínez-García, A., Sigman, D. M., Ren, H., Anderson, R., Straub, M., Hodell, D., Jaccard, S., Eglinton, T. I., and Haug, G.
        H.:   Iron   fertilization   of   the   subantarctic   ocean   during   the   last   ice   age,   Science,   343,   1347–1350,
        https://doi.org/10.1126/science.1246848, 2014.

       Mauritsen, T., Bader, J., Becker, T., Behrens, J., Bittner, M., Brokopf, R., Brovkin, V., Claussen, M., Crueger, T., Esch, M.,
        Fast, I., Fiedler, S., Fläschner, D., Gayler, V., Giorgetta, M., Goll, D. S., Haak, H., Hagemann, S., Hedemann, C.,
615   Hohenegger, C., Ilyina, T., Jahns, T., Jimenéz-de-la Cuesta, D., Jungclaus, J., Kleinen, T., Kloster, S., Kracher, D., Kinne,
        S., Kleberg, D., Lasslop, G., Kornblueh, L., Marotzke, J., Matei, D., Meraner, K., Mikolajewicz, U., Modali, K., Möbis, B.,
        Müller, W. A., Nabel, J. E., Nam, C. C., Notz, D., Nyawira, S. S., Paulsen, H., Peters, K., Pincus, R., Pohlmann, H., Pongratz,
        J., Popp, M., Raddatz, T. J., Rast, S., Redler, R., Reick, C. H., Rohrschneider, T., Schemann, V., Schmidt, H., Schnur, R.,

Climate
of the Past
Discussions

Open Access

EGU

Schulzweida, U., Six, K. D., Stein, L., Stemmler, I., Stevens, B., von Storch, J. S., Tian, F., Voigt, A., Vrese, P., Wieners,
620   K. H., Wilkenskjeld, S., Winkler, A., and Roeckner, E.: Developments in the MPI-M Earth System Model version 1.2 (MPI-
       ESM1.2) and Its Response to Increasing CO_2, Journal of Advances in Modeling Earth Systems 11, 998–1038,
       https://doi.org/10.1029/2018MS001400, 2019.

Menviel, L. (2019). The southern amplifier. Science, 363, 1040–1041. https://doi.org/10.1126/science.aaw7196

Mitsui, T., Willeit, M., Boers, N.: Synchronization phenomena observed in glacial–interglacial cycles simulated in an Earth
625   system model of intermediate complexity, Earth Syst. Dynam. 14, 1277–1294, https://doi.org/10.5194/esd-14-1277-2023,
       2023.

Niu, L., Lohmann, G., Hinck, S., Gowan, E. J., and Krebs-Kanzow, U.: The sensitivity of Northern Hemisphere ice sheets to
       atmospheric forcing during the last glacial cycle using PMIP3 models, J. Glaciol., 65, 645–661,
       https://doi.org/10.1017/jog.2019.42, 2019.

630   NSIDC: IceBridge BedMachine Greenland, Version 1, NSICDC [data set], https://doi.org/10.5067/5XKQD5Y5V3VN, 2024.

Ohgaito, R., Yamamoto, A., Hajima, T., O'ishi, R., Abe, M., Tatebe, H., Abe-Ouchi, A., Kawamiya, M.: PMIP4 experiments
       using MIROC-ES2L Earth system model, Geosci. Model Dev. 14, 1195–1217, https://doi.org/10.5194/gmd-14-1195-2021,
       2021.

Ohmura, A., Calanca, P., Wild, M. and Anklin M.: Precipitation, accumulation and mass balance of the Greenland Ice sheet,
635   Z. Gletscherkd. Glazialgeol., 35(1), 1–20, 1999.

Paillard, D.: The timing of Pleistocene glaciations from a simple multiple-state climate model, Nature, 391, 378–381,
       https://doi.org/10.1038/34891, 1998.

Parrenin, F. and Paillard, D.: Amplitude and phase of glacial cycles from a conceptual model, Earth Planet. Sc. Lett., 214,
       243–250, 2003.

640   Peltier, W. R., Argus, D. F., and Drummond, R.: Space geodesy constrains ice age terminal deglaciation: The global
       ICE6G_C(VM5a) model, J. Geophys. Res.-Solid, 120, 450–487, https://doi.org/10.1002/2014JB011176, 2015.

Pena, L. D. and Goldstein, S. L.: Thermohaline circulation crisis and impacts during the mid-Pleistocene transition, Science,
       345, 318–322, https://doi.org/10.1126/science.1249770, 2014.

Portier, A. M., Thierens, M., Martin, E. E., Hemming, S. R., Gombiner, J. H., and Raymo, M. E.: Late Pleistocene emergence
645   of crystalline Canadian Shield sources in sediments of the northern Gulf of Mexico, Paleoceanography and Paleoclimatology
       36, e2020PA004082, https://doi. org/10.1029/2020PA004082, 2021.

Qin, B., Jia, Q., Xiong, Z., Li, T., Algeo, T. J. and Dang, H.: Sustained Deep Pacific carbon storage after the Mid-Pleistocene
       Transition linked to enhanced Southern Ocean stratification, Geophys. Res. Lett. 49, e2021GL097121,
       https://doi.org/10.1029 /2021GL097121, 2022.

650   Quiquet, A., Dumas, C., Paillard, D., Ramstein, G., Ritz, C., and Roche, D. M.: Deglacial Ice Sheet Instabilities Induced by
       Proglacial Lakes, Geophys. Res. Lett., 48, e2020GL092141, https://doi.org/10.1029/2020GL092141, 2021.

Roe, G. H. and Lindzen, R. S.: The Mutual Interaction between Continental-Scale Ice Sheets and Atmospheric Stationary Waves, J. Climate, 14, 1450–1465, 2001.

Roy, M., Clark, P. U., Raisbeck, G. M., and Yiou, F.: Geochemical constraints on the regolith hypothesis for the middle
655   Pleistocene transition, Earth and Planetary Science Letters, 227, 281–296, https://doi.org/10.1016/j.epsl.2004.09.001, 2004.

Saini, H., Meissner, K. J., Menviel, L., and Kvale, K.: Impact of iron fertilisation on atmospheric CO_2 during the last glaciation, Clim. Past, 19, 1559–1584, https://doi.org/10.5194/cp-19-1559-2023, 2023.

Scherrenberg, M. D. W., Berends, C. J., Stap, L. B., and van de Wal, R. S. W.: Modelling feedbacks between the Northern Hemisphere ice sheets and climate during the last glacial cycle, Clim. Past, 19, 399–418, https://doi.org/10.5194/cp-19-399-
660   2023, 2023.

Scherrenberg, M. D. W., Berends, C. J., and van de Wal, R. S. W.: Late Pleistocene glacial terminations accelerated by proglacial lakes, Clim. Past, 20, 1761–1784, https://doi.org/10.5194/cp-20-1761-2024, 2024.

Shi, X., Werner, M., Yang, H., D'Agostino, R., Liu, J., Yang, C., Lohmann, G.: Unraveling the complexities of the Last Glacial Maximum climate: the role of individual boundary conditions and forcings, Clim. Past 19, 2157–2175,
665   https://doi.org/10.5194/cp-19-2157-2023, 2023.

Sigman, D. M., Boyle, E. A.: Glacial/interglacial variations in atmospheric carbon dioxide. Nature, 407, 859–869. https://doi.org/10.1038/35038000, 2000

Sigman, D. M., Hain, M. P., Haug, G. H.: The polar ocean and glacial cycles in atmospheric CO_2 concentration. Nature, 466, 47–55. https://doi.org/10.1038/nature09149, 2010

670 Spratt, R. M. and Lisiecki, L. E.: A Late Pleistocene sea level stack, Clim. Past, 12, 1079–1092, https://doi.org/10.5194/cp-12-1079-2016, 2016.

Tabor, C. R., Poulsen, C. J., and Pollard, D.: How obliquity cycles powered early Pleistocene global ice-volume variability, Geophys. Res. Lett., 42, 1871–1879, https://doi.org/10.1002/2015GL063322, 2015.

Tabor, C. R. and Poulsen, C. J.: Simulating the mid-Pleistocene transition through regolith removal, Earth Planet. Sc. Let.,
675   434, 231–240, https://doi.org/10.1016/j.epsl.2015.11.034, 2016.

Thomas, N. C., Bradbury, H. J., Hodell, D. A., 2022. Changes in North Atlantic deep-water oxygenation across the Middle Pleistocene Transition. Science 377, 654–659, https://doi.org/10.1126/science.abj7761

Tzedakis, P. C., Crucifix, M., Mitsui, T., and Wolff, E. W.: A simple rule to determine which insolation cycles lead to interglacials, Nature, 542, 427–432, https://doi.org/10.1038/nature21364, 2017.

680 Volodin, E. M., Mortikov, E. V., Kostrykin, S. V., Galin, V. Y., Lykossov, V. N., Gritsun, A. S., Diansky, N. A., Gusev, A. V., Iakovlev, N. G., Shestakova, A. A., and Emelina, S. V.: Simulation of the modern climate using the INM-CM48 climate model. Russ. J. Numer. Anal. M 33, 367–374. https://doi.org/10.1515/rnam-2018-0032, 2018

Watanabe, Y., Abe-Ouchi, A., Saito, F., Kino, K., O'ishi, R., Ito, T., Kawamura, K., and Chan, W.-L.: Astronomical forcing shaped the timing of early Pleistocene glacial cycles, Communications Earth & Environment, 4, 2023.

685 Willeit, M., Ganopolski, A., Calov, R., and Brovkin, V.: Mid-Pleistocene transition in glacial cycles explained by declining CO_2 and regolith removal, Sci. Adv., 5, eaav7337, https://doi.org/10.1126/sciadv.aav7337, 2019.

Yamamoto, M., Clemens, S. C., Seki, O., Tsuchiya, Y., Huang, Y., O'ishi, R., and Abe-Ouchi, A.: Increased interglacial atmospheric CO_2 levels followed the mid-Pleistocene Transition, Nat. Geosci., 15, 307–313, https://doi.org/10.1038/s41561-022-00918-1 2022.

690 Zwally, H. J. and Giovinetto, M. B.: Areal distribution of the oxygen-isotope ratio in Greenland, Ann. Glaciol., 25, 208–213, https://doi.org/10.3189/S0260305500014051, 1997.